Above-Threshold Ionization by an Elliptically Polarized Field: Interplay between Electronic Quantum Trajectories

G. G. Paulus, F. Grasbon, A. Dreischuh,* and H. Walther†
Max-Planck-Institut für Quantenoptik, 85748 Garching, Germany

R. Kopold and W. Becker‡
Max-Born-Institut, 12489 Berlin, Germany
(Received 9 December 1999)

Measurements of energy-resolved angular distributions of electrons generated in above-threshold ionization of rare gases in a field with elliptical polarization are presented, with emphasis on the high-energy part of the spectra. The data show a second plateau at a specific angle with respect to the large component of the laser field. The results are compared to a calculation based on a strong-field rescattering approximation. This is interpreted in terms of the superposition of quantum trajectories. The second plateau is associated with the interference of electrons that do and that do not rescatter.

PACS numbers: 32.80.Rm

Since its discovery 20 years ago [1], above-threshold ionization (ATI), i.e., ionization such that the atom absorbs more photons from the laser field than necessary, has kept revealing surprising facets. Some basic features of ATI are largely independent of the atomic species. They include a cutoff in the electron's energy spectrum at low energy, another one at high energy, and a plateau in between, as well as the angular dependence of these cutoffs. (For a review, see Ref. [2].) These features appear the more clearly, the higher the intensity of the applied laser field. Other features are atom specific and better developed at medium-high intensity; for example, spectra recorded for argon exhibit enhancements of particular groups of ATI peaks at medium to high energies that appear to be absent for other rare gases [3,4]. The former group of effects can be well understood in terms of what is called the simple-man model [5–7], while the origin of the last-mentioned findings is still under discussion [8]. One of the fascinating aspects of ATI is the interplay of atomic physics and large-scale, almost mesoscopic, free-electron motion in the laser field. While ATI has been of academic interest thus far, its twin effect, high-harmonic generation (HHG), promises to yield novel sources of radiation with unprecedented properties [9]. HHG is governed by much the same physics as ATI.

Elliptical polarization of the incident laser field literally adds a new dimension to ATI. In this Letter, the first systematic measurements of angular-resolved above-threshold ionization electron spectra are presented up to energies around the end of the plateau and beyond. Unexpectedly and in marked contrast to the case of linear polarization, the angular distributions in this energy region are highly structured. We will interpret these structures as interferences of two different kinds of quantum trajectories, associated with "direct" and with "rescattered" electrons. The quantum trajectories constitute a quantum extension of the electron orbits of the aforementioned classical simple-man model. They have been instrumental in the analysis of HHG [10] where the contributions of particular quantum paths to the collective response have been experimentally observed [11] and theoretically analyzed [12,13]. Interference of quantum trajectories is a phenomenon well known from theoretical simulations [10,12–14]. Experimentally, however, interferences are difficult to detect as they tend to be washed out by focal averaging. Ellipticity has been of help here before, and interferences of low-energy direct ATI electrons as a function of the laser ellipticity have recently been observed [15], but with rather low contrast. The interferences we will report here are more subtle as they involve both the direct and the rescattered electrons and at the same time exhibit high contrast. Our work augments earlier interesting data, including angular distributions, of low-energy ATI by an elliptically polarized field [16].

Let us briefly review the simple-man model for a linearly polarized field. In a visualization of ATI, we discriminate between direct and rescattered electrons. Both are generated by tunneling and appear in the continuum at some instant t' with zero velocity. The former leave the range of the atomic binding potential without much additional interaction with it. The latter are accelerated by the laser field away from the ion and then back to it. In the ensuing encounter at time t they may rescatter and backscatter (or recombine in the case of HHG). The simple-man model describes the electronic motion for times between t' and t and for times later than t by simple classical orbits neglecting the binding potential. It predicts cutoff energies for the direct and the rescattered electrons of $2U_p$ and $10U_p$, respectively. (U_p denotes the ponderomotive energy which is the quiver energy of an electron in an oscillating electrical field.)

This simple classical model, however, has its limits. First, it is unclear how to extend it to elliptical polarization since electrons that start with zero velocity never return to their starting point. Second, interference effects, being quantum mechanical, are beyond its scope. Whenever

different pathways exist by which the electron reaches its (given) final state, the constructive or destructive interference of these pathways determines the detailed form of the spectra.

The pathways that interfere are particularly simple in the case of a zero-range binding potential. Formally, they originate from a saddle-point analysis of the S-matrix element in a Keldysh approximation suitably improved such that rescattering is accounted for [17]. They are essentially the simple-man orbits mentioned above, each parametrized by its start time t', return time t, and canonical momentum $\mathbf{k}$ of the orbit in between. However, in contrast to the simple-man orbits, the more elaborate analysis assigns small imaginary parts to these parameters which are related to the electron's origin through tunneling. Moreover, the electron does not necessarily start with zero velocity. Details can be found elsewhere [18]. For a given final momentum $\mathbf{p}$, there are several such orbits, numbered by the subscript n, and the S-matrix element for ionization can be represented in the form

$$M_{\mathbf{p}} = \sum_n (\det S''_{\mathbf{p},n})^{-1/2} \exp[iS_{\mathbf{p}}(t_n, t'_n, \mathbf{k}_n)]. \qquad (1)$$

The quantity $S_{\mathbf{p}}(t_n, t'_n, \mathbf{k}_n)$ is the action evaluated along the above-mentioned orbit, and $S''_{\mathbf{p},n}$ denotes the (five-dimensional) matrix of its second derivatives, evaluated for $t_n, t'_n, \mathbf{k}_n$ [14]. The representation (1) looks like an approximation to the quantum mechanical path integral and, in fact, it is. It vividly illustrates the interference of the various orbits. All of the interpretations we give are based on the quantum path representation (1) while the explicit results have been calculated from the improved Keldysh approximation [17] that underlies Eq. (1).

We are primarily interested in high-precision data of the plateau electrons. However, their contributions are dwarfed by those of the direct electrons by more than 2 orders of magnitude. In order to avoid space charge effects we have to restrict the electron count rate to a few electrons per laser shot and thus to *very* few plateau electrons per laser shot. This calls for using high-repetition-rate lasers. We have used two such systems. Both deliver intensities up to 10^{14} W/cm^2 with a pulse duration below 50 fs. They differ in wavelength (630 and 800 nm) and repetition rate (6.2 and 100 kHz). The ellipticity of the laser polarization and the orientation of the polarization ellipse are controlled with an achromatic quarter- and half-wave plate, respectively. Lenses achromatized around the respective central wavelengths are used to focus the laser beam into the interaction region. Perpendicular to the laser beam the target gas is directed into the focus via a nozzle with an opening diameter of only 5 μm. This is more than 10 times smaller than the Rayleigh length of the focus and therefore reduces the problem of averaging the photoelectron spectra that originate from the various intensities in the focus. The kinetic energy of the photoelectrons is measured by means of the time-of-flight method. Because of the high repetition rate an extremely efficient method for measuring the flight times had to be developed. At the heart of this system is a PC-hosted multiscaler (FAST 7886) with a clock rate of 2 GHz which is programmed in assembler code and can handle up to two photoelectrons per laser shot on the average without sacrificing a single shot.

We measure a photoelectron angular distribution (AD) for fixed ellipticity by successively adjusting the orientation of the polarization ellipse to 145 different angles in a range of 360° and by recording the corresponding ATI spectra. About 10^8 electrons are necessary for an AD of reasonable quality. To present a survey of the ADs of the photoelectrons, the data are plotted as a gray-scale density plot, Fig. 1, and as a shaded surface plot, Fig. 2. Electrons registered in the direction of the large axis of the polarization ellipse are assigned an angle of 0°. Because of the inversion symmetry of the ADs, the data are plotted from $-90°$ to $+90°$ only.

For linear polarization ($\xi = 0$) the angular distribution is symmetric with respect to the large (as well as the small) axis of the polarization ellipse. This fourfold symmetry is lost as soon as some ellipticity ($\xi \neq 0$) is introduced to the laser polarization. Inversion symmetry, however, is preserved. At an electron energy above 25 eV, which coincides with the onset of the ATI plateau, the appearance of the ADs changes abruptly, confirming the different mechanisms behind the creation of photoelectrons with low and high energy. The ADs are still asymmetric, although much less pronounced. As compared to the case of linear polarization, the plateau electrons are now emitted at some angle away from the large axis of the polarization.

The most interesting feature of the angular distributions presented in Figs. 1 and 2 is a second ATI plateau. It manifests itself as a ridge parallel to the more intense ridge

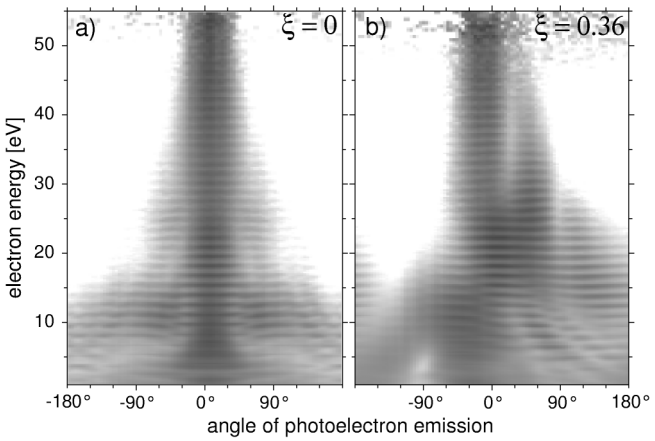

FIG. 1. Density plots of the energy-resolved angular distribution for Xe at an intensity of 7.7×10^{13} W/cm^2 and a wavelength of 800 nm for an ellipticity of $\xi = 0$ (a) and $\xi = 0.36$ (b). 0° corresponds to electrons emitted in the direction of the main axis of the polarization ellipse. Dark means high electron yield. For visual convenience the data were normalized for each ATI peak.

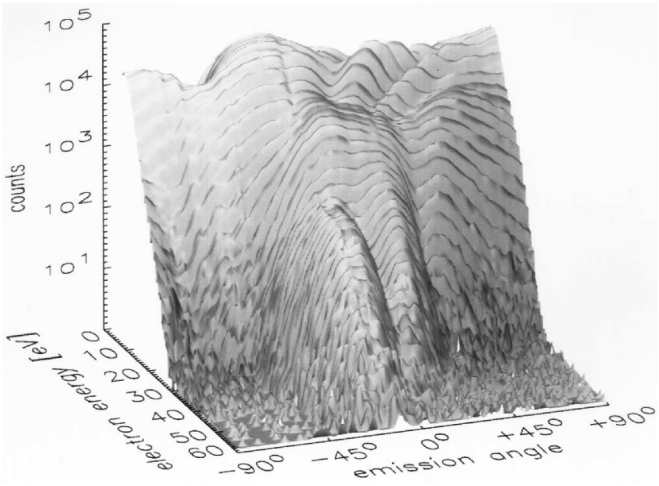

FIG. 2. Shaded surface plot of the same measurement as in Fig. 1(b). The dark stripes parallel to the angle axis correspond to the ATI peaks. The two plateaus are clearly visible.

that represents the original plateau. In the density plot, Fig. 1(b), the ridges appear as dark stripes. At lower energies this second plateau shifts to larger angles. In addition, other ridges appear parallel to the second plateau. This feature is present for both laser wavelengths and for all species of rare gases under investigation, namely Ne, Ar, and Xe, although with different intensity and at different angles. The appearance of this second plateau is very unusual. In all cases investigated thus far, the ADs beyond the cutoff ($10U_p$ at 0°) exhibit just one smooth peak, in agreement with the theoretical idea that they are dominated by one single trajectory, the one with the highest cutoff.

For a physical explanation of the second plateau, we turn to the quantum path representation (1) of the S-matrix element. The paths that need be considered include direct and rescattered electrons. It is expedient, both conceptually and from a calculational point of view, to display and treat them separately, so that $M_{\mathbf{p}} = M_{\mathbf{p}}^{(0)} + M_{\mathbf{p}}^{(1)}$. The direct part

$$M_{\mathbf{p}}^{(0)} = \sum_n (S''_{\mathbf{p},n})^{-1/2} \exp[iS_{\mathbf{p}}(t_n)] \qquad (2)$$

includes the quantum orbits such that the electron leaves the ion without additional interaction. Hence, it is just specified by the (complex) time t_n of ionization, and the action $S_{\mathbf{p}}(t_n)$ is calculated along this direct path. The rescattered part $M_{\mathbf{p}}^{(1)}$ has the form (1), except that the paths with short travel times $t_n - t'_n$ are to be omitted from the sum [19].

Figure 3(a) displays ADs calculated from Eq. (1) for various ATI orders s in the rescattering region. For comparison, experimental results are plotted in Fig. 3(b). They correspond to cuts of Fig. 1(b) at the respective electron energies. The most pronounced features shared by experiment and theory are the two well developed maxima on either side of 0° and the minimum in between, at a very

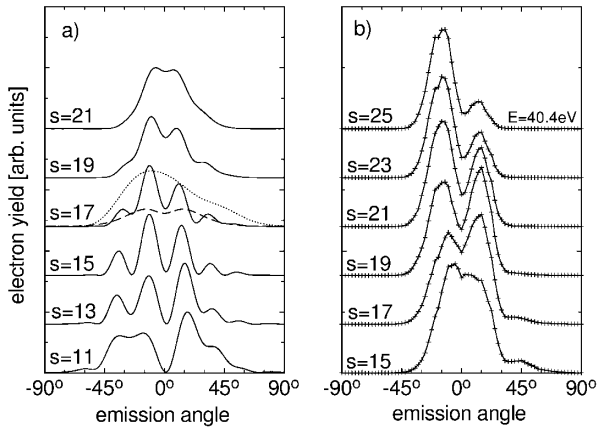

FIG. 3. Calculated (a) and measured (b) angular distributions of various ATI peaks in the plateau region. In addition, in panel (a) the amplitudes for the direct electrons (dashed) and the rescattered electrons (dotted) are plotted for the ATI order $s = 17$. The photon energy is $\approx$1.55 eV. The experimental result was obtained by performing cuts of Fig. 1 at the respective energies. The curves are normalized and separated in the vertical direction for visual convenience. The parameters are the binding energy of 0.436 a.u. (just below the binding energy of xenon, in order to stay away from a channel closing), an intensity of 5.7×10^{13} W/cm^2 somewhat below the peak intensity of the experiment, and an ellipticity of $\xi = 0.48$, larger than in the experiment.

small positive angle. In Figs. 1 and 2, they can be recovered as the two parallel ridges (the two plateaus) and the valley in between. The angular positions of all three hardly depend on the energy. For the interpretation of these spectral features we consider the separate contributions of the direct electrons ($|M_{\mathbf{p}}^{(0)}|$, dashed line) and the rescattered electrons ($|M_{\mathbf{p}}^{(1)}|$, dotted line) which are given in Fig. 3(a) for $s = 17$. Neither one shows any pronounced angular dependence; their coherent sum $|M_{\mathbf{p}}^{(0)} + M_{\mathbf{p}}^{(1)}|$, however, does. Hence, the effect is caused by the interference of these two contributions. Notice that as expected for this energy range the rescattered electrons (dotted line) are clearly dominant. Their contribution is very smooth and not much different from a corresponding AD for linear polarization; cf. Fig. 1(a). It is remarkable how clear the consequences of quantum path interference are in the rescattering region under these conditions. The contrast of the interference pattern in the measurement reaches 0.5. The theoretical results have been calculated for fixed intensity. They exhibit additional, less well developed, interferences that are not shared by the data. Most likely they have been washed out by focal averaging.

Interference of direct and rescattered electrons has nothing, in principle, to do with the ellipticity of the polarization. However, whether or not it has visible consequences depends in a very subtle fashion on the behavior of the yields of the direct and of the rescattered electrons as a function of energy. It is only for sufficiently high ellipticity and moderate intensity that the yields remain comparable over an extended energy range, thus allowing

for sufficient contrast in the interference pattern. Compared to the case of linear polarization, this is caused by a reduced yield of the rescattered electrons. Quantitatively, these features depend on the choice of the binding potential. Therefore, our theory correctly predicts the observed patterns and their trends, though not exactly where they are observed as a function of the parameters.

The quantum path interpretation of the theoretical calculations presents an appealing physical picture of the mechanism behind the observed second plateau. It also makes predictions that can be tested in future experiments: for example, with increasing intensity, the second plateau will retreat to higher ellipticities and finally disappear. A quantitative comparison between experiment and theory has not been attempted for the reasons mentioned above and in view of some approximations inherent in the theory of which the Keldysh approximation is the most important, even though it has been modified to allow for rescattering [20]. The Keldysh approximation is known to yield (for any potential and any polarization) a fourfold symmetry for the ADs of the direct electrons, in contrast to experiments for elliptical polarization [16]. The experimentally observed violation of this symmetry is due to the combined effect of the field and the binding potential [21–23]. Rescattering already constitutes such a combined effect and, consequently, in the rescattering regime our theory also violates the fourfold symmetry. We expect that the rescattered electrons are not overly sensitive to the shape of the binding potential for which we took a zero-range potential. However, the insufficient description of the direct electrons will affect the exact positions of the interference maxima and minima.

In conclusion, we have measured angular distributions of ATI photoelectrons in the plateau regime. For elliptical polarization, the plateau electrons are emitted at a nonzero angle with respect to the large axis of the laser field, which is independent of the energy. In addition, a remarkably well developed effect stands out: this is a second ATI plateau, again at a constant angle, which is separated from the first by approximately 30°. By comparison with a Keldysh-type theory we suggest that this effect is due to the interference of two pathways for ionization: the electron may leave the ionic core either directly or after an additional interaction with the atomic potential. This implies that the angular position of the second plateau is not amenable to classical models. The observation of the second plateau in qualitative agreement with the calculations lends additional support to the quantum orbit picture of intense-laser atom physics phenomena and confirms its predictive power.

This work was supported in part by the Deutsche Forschungsgemeinschaft. A. D. thanks the Alexander-von-Humboldt-Stiftung.

*Permanent address: Sofia University, Dept. of Quant. Elect., 5 J. Bourchier Blvd., BG-1164 Sofia, Bulgaria.
†Also at Sektion Physik der Ludwig-Maximilians-Univ. München, Am Coulombwall 1, 85747 Garching, Germany.
‡Also at Center for Advanced Studies, Dept. of Phys. and Astr., Univ. of New Mexico, Albuquerque, NM 87131.

[1] P. Agostini *et al.,* Phys. Rev. Lett. **42**, 1127 (1979).
[2] L. F. DiMauro and P. Agostini, Adv. At. Mol. Opt. Phys. **35**, 79 (1995).
[3] M. P. Hertlein *et al.,* J. Phys. B **30**, L197 (1997).
[4] P. Hansch *et al.,* Phys. Rev. A **55**, R2535 (1997).
[5] H. B. v. Linden v. d. Heuvell and H. G. Muller, in *Multiphoton Processes,* Studies in Modern Optics Vol. 8 (Cambridge University Press, Cambridge, 1988), p. 25.
[6] P. B. Corkum, Phys. Rev. Lett. **71**, 1994 (1993).
[7] G. G. Paulus *et al.,* Phys. Rev. A **52**, 4043 (1995).
[8] M. J. Nandor *et al.,* Phys. Rev. A **60**, R1771 (1999).
[9] Ch. Spielmann *et al.,* Nature (London) **278**, 661 (1997).
[10] M. Lewenstein *et al.,* Phys. Rev. A **51**, 1495 (1995).
[11] M. Bellini *et al.,* Phys. Rev. Lett. **81**, 297 (1998).
[12] M. B. Gaarde *et al.,* Phys. Rev. A **59**, 1367 (1999).
[13] Ph. Balcou *et al.,* J. Phys. B **32**, 2973 (1999).
[14] R. Kopold *et al.,* Opt. Commun. (to be published).
[15] G. G. Paulus *et al.,* Phys. Rev. Lett. **80**, 484 (1998).
[16] M. Bashkansky *et al.,* Phys. Rev. Lett. **60**, 2458 (1988).
[17] A. Lohr *et al.,* Phys. Rev. A **55**, R4003 (1997).
[18] R. Kopold *et al.* Phys. Rev. Lett. **84**, 3831 (2000).
[19] The quantum paths with short travel times cannot be evaluated directly from Eq. (1). They are subsumed into the term $M_{\mathbf{p}}^{(0)}$ of Eq. (2). Details of this procedure will be explained elsewhere.
[20] A numerical solution of the three-dimensional time-dependent Schrödinger equation for elliptical polarization with an accuracy sufficient for high-order ATI would be very demanding; cf. M. Protopapas *et al.,* Phys. Rev. Lett. **79**, 4550 (1997); see also H. G. Muller, Phys. Rev. A **60**, 1341 (1999), for linear polarization.
[21] H. G. Muller *et al.,* Phys. Rev. Lett. **61**, 2507 (1988), and references therein.
[22] W. Becker *et al.,* Laser Phys. **8**, 56 (1998).
[23] Using Coulomb-Volkov solutions in the context of the Keldysh approximation already produces strong violations of the fourfold symmetry; see A. Jaroń *et al.,* Opt. Commun. **163**, 115 (1999).